J. Fluid Mech. (1989), *vol.* 207, *pp.* 73–96
Printed in Great Britain

Nonlinear evolution of oblique waves on compressible shear layers

By M. E. GOLDSTEIN[1] AND S. J. LEIB[2]

[1] National Aeronautics and Space Administration, Lewis Research Center, Cleveland, OH 44135, USA

[2] Sverdrup Technology, Inc. Lewis Research Center Group, NASA Lewis Research Center, Cleveland, OH 44135, USA

(Received 15 August 1988)

We consider the effects of critical-layer nonlinearity on spatially growing oblique instability waves on compressible shear layers between two parallel streams. The analysis shows that mean temperature non-uniformities cause nonlinearity to occur at much smaller amplitudes than it does when the flow is isothermal. The nonlinear instability wave growth rate effects are described by an integro–differential equation which bears some resemblance to the Landau equation in that it involves a cubic-type nonlinearity. The numerical solutions to this equation are worked out and discussed in some detail. We show that inviscid solutions always end in a singularity at a finite downstream distance but that viscosity can eliminate this singularity for certain parameter ranges.

1. Introduction

There has recently been a resurgence of interest in understanding the stability characteristics of supersonic mixing layers (Papamoshou & Roshko 1986, 1988; Jackson & Grosch 1988; Tam & Hu 1989). The primary motivation seems to come from its potential application to the control of mixing in hypersonic propulsion systems (Kumar, Bushnell & Hussaini 1987).

Harmonic excitation of free shear layers between parallel streams produces a monochromatic spatially growing instability wave that is initially governed by linear dynamics for sufficiently small excitation amplitudes. The excitation frequency is usually chosen so that the initial instability wave growth rate is near the maximum for the shear layer at the excitation position so that viscous shear layer spreading produces a gradual reduction in the local growth rate even though the instability wave amplitude continues to increase. Nonlinear effects can then become important in a 'critical layer' at the transverse position where the mean flow and instability wave phase velocities are equal (once the instability wave amplitude becomes sufficiently large and its growth rate becomes sufficiently small). The unsteady critical-layer flow is then governed by a nonlinear vorticity equation, while the motion outside the critical layer remains essentially linear. The external instability wave growth rate is, however, completely controlled by the nonlinear dynamics of the critical layer.

Goldstein & Leib (1988) and Goldstein & Hultgren (1988) analysed this phenomenon for an incompressible (and therefore subsonic) shear layer. They consider only a two-dimensional flow, since the two-dimensional instability is the

most rapidly growing linear mode in that case. In this paper, we analyse the corresponding problem for compressible shear layers in which oblique modes can grow faster than the two-dimensional mode if the Mach number is sufficiently large (Gropengeisser 1969). The analysis must therefore be extended to the three-dimensional case. The calculated reduction in linear growth rates with increasing Mach number (Gropengeisser 1969) suggests that nonlinear critical layer effects will be correspondingly more important in supersonic flows. Goldstein & Leib (1988) and Goldstein & Hultgren (1988) show that two-dimensional critical-layer nonlinearity occurs at the downstream position where the deviation of the local thickness Strouhal number, or normalized frequency, from its neutral value is $O(\epsilon^{\frac{1}{2}})$, where $\epsilon \ll 1$ is the small local instability wave amplitude. The latter analysis, which includes viscous effects within the critical layer, shows that even very small viscosity eventually causes the critical layer to evolve into a quasi-equilibrium critical layer similar to the one originally considered by Benney & Bergeron (1969).

The present analysis shows that the critical-layer nonlinearity behaves quite differently for non-isothermal flows – primarily because (as pointed out by Reshotko 1960) the temperature fluctuations have an algebraic singularity in the critical layer and therefore become very large relative to the remaining velocity components in the plane of the wave. This causes the critical-layer nonlinearity to occur at a much smaller amplitude *vis-à-vis* the two-dimensional isothermal case. In fact, nonlinearity now becomes important when the instability wave growth rate is $O(\epsilon^{\frac{2}{5}})$. Hickernell (1984), who considered temporally growing Rossby waves in the beta-plane approximation, found a similar scaling for critical layers associated with certain singular neutral modes.

This change in scaling relative to the two-dimensional isothermal case produces a corresponding change in critical-layer structure. The critical-layer flow is now governed by linear dynamics to lowest order of approximation, with nonlinearity entering only through the higher-order (inhomogeneous) terms. The instability wave growth rate is still completely controlled by the nonlinear terms, but can now be calculated from an amplitude equation similar to the one found by Hickernell (1984) for the Rossby wave singular modes – even though our critical-layer vorticity distribution is quite different from his.

The amplitude equation can be normalized so that its solutions depend on two real parameters, one of which is related to the scaled growth rate of the linear instability wave entering the nonlinear region, while the other can be thought of as a normalized temperature gradient. The resulting normalized equation still has to be solved numerically. This is accomplished by using a fourth-order predictor–corrector scheme to integrate in the downstream direction, starting from the upstream linear state which is prescribed far upstream in the flow (relative to the streamwise lengthscale of the nonlinear region).

The calculated instability wave amplitudes initially follow the prescribed linear growth, but soon begins to either saturate or increase their rate of growth when the nonlinear effects come into play. Cumulative history effects eventually counteract these trends, causing a rapid increase in amplitude which ends in a singularity at a finite downstream distance in the inviscid case. An equilibrium solution exists for certain parameter ranges in the viscous case. We obtain asymptotic solutions (to the amplitude equation) for each of these cases. The problem was rescaled in the immediate vicinity of the singularity in the singular case in order to obtain the local asymptotic solution, which suggests that the flow will become fully nonlinear

everywhere in the shear layer and that the motion will then be governed by the full three-dimensional Euler's equations. This will be pursued in a forthcoming paper.

The overall plan of the paper is as follows. The problem is formulated in §2, where we show how the nonlinear critical layer gradually evolves from the strictly linear finite-growth-rate solution. A general compressible shear layer with arbitrary mean temperature profile is considered, but we restrict the analysis of the unsteady flow to the inviscid case. The flow outside the critical layer is a linear, unsteady three-dimensional perturbation about the two-dimensional mean shear-layer flow, which can be treated as locally parallel on the streamwise lengthscale over which the nonlinear effects take place. The latter occur entirely within the critical layer to the order of approximation of the analysis and determine the unknown amplitude function in the external solution. The pressure fluctuation is taken as the basic variable for the external flow, and the (linear) equation for this quantity is expressed in terms of 'Squire coordinates' in the directions along and perpendicular to the propagation direction of the wave, which causes it to be independent of its 'spanwise' transverse coordinate.

We introduce a 'slowly varying' amplitude function, which is ultimately determined by the nonlinear flow in the critical layer, which we analyse in §3. Squire coordinates are again used for the independent variables, but spanwise vorticity and temperature are now used for the dependent variables.

The solution that matches onto the upstream linear solution and onto the linear solution outside the critical layer is then found by sequential integration of the resulting first-order partial differential equations. Matching with the linear external instability wave leads to a Hickernell (1984)-type equation that determines the amplitude of that wave. In §4 we obtain an asymptotic solution of this equation that is valid in the vicinity of the singularity. Viscous effects are discussed in §5 where the viscous amplitude evolution equation is derived and an asymptotic solution to the latter is obtained. A discussion of the numerical solutions to these equations and comparison with the asymptotic solutions is given in §6.

2. Formulation and solution outside the critical layer

We are concerned with a nearly inviscid compressible shear flow of an ideal gas between two parallel streams with nominally uniform temperatures $T^{(1)}, T^{(2)}$ and velocities $U^{(1)} > U^{(2)}$. The upstream flow consists of an oblique (i.e. three-dimensional) spatially growing (i.e. time harmonic) instability wave on the steady two-dimensional shear layer that forms between the two streams.

The flow parameters in the high-speed stream are used as reference quantities and are generally denoted by the superscript 1. The reference length, say δ, is taken to be some suitable thickness of the mean shear layer (e.g. momentum thickness). Then the steady flow is characterized by the Mach number

$$M \equiv U^{(1)}/C^{(1)} \tag{2.1}$$

and Reynolds number

$$Re \equiv U^{(1)}\delta/\nu^{(1)}, \tag{2.2}$$

where

$$C^{(1)} = (k\mathscr{R}T^{(1)})^{\frac{1}{2}} \tag{2.3}$$

is the speed of sound in the high speed stream, ν is the kinematic viscosity, k is the isentropic exponent of the gas, and $\mathscr{R}$ is the gas constant.

We suppose that Re is large enough that the mean pressure is constant across the

shear layer and that the mean flow is nearly parallel over many wavelengths of the linear instability wave.

Then the local mean density R_0 and mean temperature T_0 are related by

$$R_0 T_0 = 1, \tag{2.4}$$

and for purposes of our analysis $T_0(y)$ can be thought of as a given (regular) function of y (see equation (2.17) below). When nonlinear effects do not first intervene, the gradual viscous spreading of the mean shear layer causes the spatial growth rate of the linear instability wave to gradually decrease (Crighton & Gaster 1976) until it approaches its neutral stability condition (i.e. point of zero growth), whose Strouhal number (i.e. frequency normalized by $\delta/U^{(1)}$) and streamwise and spanwise wavenumbers we denote by S_0, α_0, and β_0 respectively.

Nonlinear effects will first become important at the streamwise position (upstream of the linear neutral stability point) where the local Strouhal number S is

$$S = S_0 + \epsilon^{\frac{2}{5}} S_1. \tag{2.5}$$

Here $S_1 < 0$ is assumed to be $O(1)$, and ϵ denotes the characteristic amplitude of the instability wave in this region. The instability wave growth rate, which is also $O(\epsilon^{\frac{2}{5}})$, is then completely determined by nonlinear critical-layer effects. Finally, we require that the origin of the spatial coordinates x, y, z, (with x in the streamwise and z in the spanwise directions) be located within this nonlinear region.

There are at least two reasonable ways of choosing the spanwise wavenumber of the upstream linear instability wave. It is sometimes assumed to be real in strictly linear analyses of spatially growing modes in order to represent waves with fixed (i.e. steady) spanwise structure. However, this involves at least two modes with the same frequency and streamwise wavenumber but with equal and opposite spanwise wavenumbers. While these waves can be treated independently in strictly linear theories, they can interact nonlinearly in a nonlinear theory of the present type and greatly complicate the analysis. It is, on the other hand, possible to generate individual oblique modes that exhibit spatial growth along their propagation directions and most of the linear analyses have been concerned with this case (Gropengeisser 1969; Jackson & Grosch 1988, etc.). We therefore restrict the present study to this case.

The pressure fluctuation of the upstream linear instability wave will then be of the form

$$\epsilon k M^2 \cos\theta \,\mathrm{Re}\, a^{\dagger} \Pi_1(y)\, \mathrm{e}^{\mathrm{i}(\bar{\alpha}\bar{\xi} - \epsilon^{\frac{2}{5}} S_1 t) - S_1 U_c' \bar{\kappa} \bar{x}_1/2},$$

where t denotes the time,

$$\bar{\alpha} \equiv (\alpha_0^2 + \beta_0^2)^{\frac{1}{2}}, \tag{2.6}$$

and

$$\theta \equiv \tan^{-1} \beta_0/\alpha_0 \tag{2.7}$$

denotes the direction of propagation of this wave relative to the mean flow direction.

$$\bar{\xi} \equiv x\cos\theta + z\sin\theta - U_c \cos\theta t \tag{2.8}$$

is a coordinate in this direction in a reference frame moving downstream with the neutral phase velocity

$$U_c \cos\theta \equiv S_0/\bar{\alpha}, \tag{2.9}$$

$$\bar{x}_1 \equiv \epsilon^{\frac{2}{5}}(x\cos\theta + z\sin\theta) \tag{2.10}$$

is a scaled coordinate in the propagation direction, and

$$\tfrac{1}{2}\mathrm{i} S_1 U_c' \bar{\kappa}$$

is a scaled complex wavenumber whose imaginary part is minus the growth rate of the *linear* near neutral instability wave. $\Pi_1(y)$ is an appropriate solution of the relevant Rayleigh's equation (for the pressure), which can be taken as the neutral solution to the required order of approximation. The complex constant $a^\dagger$ is a measure of the complex scaled amplitude of the wave.

It is convenient to work in the oblique moving coordinate system $\{\bar{\xi}, y, \bar{z}\}$, where

$$\bar{z} = -x\sin\theta + z\cos\theta. \tag{2.11}$$

The velocity components $\{\bar{u}, v, \bar{w}\}$ in these coordinates are related to the velocity components $\{u, v, w\}$ in the original $\{x, y, z\}$ coordinates by

$$\bar{u} = u\cos\theta + w\sin\theta - U_c\cos\theta, \tag{2.12}$$

$$\bar{w} = -u\sin\theta + w\cos\theta. \tag{2.13}$$

The instability wave continues to behave linearly outside the critical layer and we expect the solution to be of the form

$$\bar{u} = \cos\theta U(y) + \epsilon\,\mathrm{Re}\,F(y)\,A^\dagger(\bar{x}_1)\,\mathrm{e}^{\mathrm{i}\bar{\alpha}\zeta} + \epsilon^{\frac{6}{5}}\bar{u}_2 + \ldots, \tag{2.14}$$

$$v = -\epsilon\bar{\alpha}\,\mathrm{Re}\,\mathrm{i}\Phi(y)\,A^\dagger(\bar{x}_1)\,\mathrm{e}^{\mathrm{i}\bar{\alpha}\zeta} + \epsilon^{\frac{6}{5}}v_2 + \ldots, \tag{2.15}$$

$$\bar{w} = -\sin\theta[U_c + U(y) - \epsilon U'(y)\,\mathrm{Re}\,\mathrm{i}\Psi(y)\,A^\dagger(\bar{x}_1)\,\mathrm{e}^{\mathrm{i}\bar{\alpha}\zeta}] + \epsilon^{\frac{6}{5}}\bar{w}_2 + \ldots, \tag{2.16}$$

$$T = T_0(y) + \epsilon\,\mathrm{Re}\,\Theta(y)\,A^\dagger(\bar{x}_1)\,\mathrm{e}^{\mathrm{i}\bar{\alpha}\zeta} + \epsilon^{\frac{6}{5}}\theta_2 + \ldots, \tag{2.17}$$

$$p = 1 + \epsilon kM^2\cos\theta\,\mathrm{Re}\,\Pi(y)\,A^\dagger(\bar{x}_1)\,\mathrm{e}^{\mathrm{i}\bar{\alpha}\zeta} + \epsilon^{\frac{6}{5}}p_2 + \ldots, \tag{2.18}$$

where $U(y) + U_c$ is the mean flow velocity,

$$\zeta \equiv \bar{\xi} - S_1\epsilon^{\frac{2}{5}}t/\bar{\alpha}, \tag{2.19}$$

and $A^\dagger$ is a function of the slow propagation direction variable $\bar{x}_1$, which will ultimately be determined by the nonlinear flow in the critical layer, but matching with the upstream linear solution requires that it satisfy the upstream boundary condition

$$A^\dagger \sim a^\dagger\,\mathrm{e}^{-S_1U_c'\bar{\alpha}\bar{x}_1/2} \quad \text{as} \quad \bar{x}_1 \to -\infty. \tag{2.20}$$

The $O(\epsilon^{\frac{6}{5}})$ terms were introduced to account for higher harmonics generated within the critical layer, but are independent of $\bar{z}$ and governed by linear dynamics outside the layer. In fact, the entire solution (2.14)–(2.18) is independent of $\bar{z}$ and satisfies linear equations to the indicated order.

The functions F, Φ, Ψ, Θ and Π of y, $\bar{x}_1$ and ϵ are determined to the required level of approximation by

$$\tilde{\alpha}^2(U-c)^2F = -T_0[\tilde{\alpha}^2(U-c)\Pi + U'\mathrm{D}\Pi], \tag{2.21}$$

$$\tilde{\alpha}^2(U-c)\Phi = -T_0\,\mathrm{D}\Pi, \tag{2.22}$$

$$\cos\theta(U-c)\Theta = T_0'\Phi + (k-1)M^2\cos^2\theta(U-c)\,T_0\,\Pi, \tag{2.23}$$

$$(U-c)^2\,\mathrm{D}\frac{T_0}{(U-c)^2}\mathrm{D}\Pi - \tilde{\alpha}^2[T_0 - M^2\cos^2\theta(U-c)^2]\,\Pi = 0, \tag{2.24}$$

where

$$\tilde{\alpha} = \bar{\alpha} + \frac{\epsilon^{\frac{2}{5}}}{\mathrm{i}A^\dagger}\frac{\mathrm{d}A^\dagger}{\mathrm{d}\bar{x}_1}, \tag{2.25}$$

$$c = \epsilon^{\frac{2}{5}}\left(\frac{S_1}{\alpha} - U_c\frac{\mathrm{d}A^\dagger/\mathrm{d}\bar{x}_1}{\mathrm{i}\bar{\alpha}A^\dagger}\right), \tag{2.26}$$

the primes denote differentiation with respect to the relevant arguments and we have put

$$\mathrm{D} \equiv \frac{\partial}{\partial y}. \tag{2.27}$$

It follows from (2.25) and (2.26) that F, Φ, Ψ, Θ and Π expand like

$$F = F_1 + \epsilon^{\frac{2}{5}} F_3 + \ldots, \quad \Pi = \Pi_1 + \epsilon^{\frac{2}{5}} \Pi_3 + \ldots \tag{2.28}$$

etc. Substituting these into (2.21) to (2.25) we find that

$$\mathrm{L}\Pi_1 = 0, \tag{2.29}$$

$$\mathrm{i}\bar{\alpha} U A^{\dagger} \mathrm{L}\Pi_3 = 2U\bar{\alpha}^2 \left(1 - \frac{M^2 U^2}{T_0} \cos^2\theta\right) \frac{\mathrm{d}A^{\dagger}}{\mathrm{d}\bar{x}_1} \Pi_1$$
$$- \sec\theta \left(U_{\mathrm{c}} \cos\theta \frac{\mathrm{d}A^{\dagger}}{\mathrm{d}\bar{x}_1} - \mathrm{i}S_1 A^{\dagger}\right) \left[\frac{1}{T_0} \frac{\mathrm{d}}{\mathrm{d}y} T_0 \frac{\mathrm{d}}{\mathrm{d}y} - \bar{\alpha}^2 \left(1 - 3 \frac{U^2 M^2}{T_0} \cos^2\theta\right)\right] \Pi_1, \tag{2.30}$$

$$\bar{\alpha}^2 F_1 = -\frac{T_0}{U} \left(\bar{\alpha}^2 \Pi_1 + \frac{U'}{U} \Pi_1'\right), \tag{2.31}$$

$$\bar{\alpha}^2 A^{\dagger} F_3 = -\frac{A^{\dagger} T_0}{U} \left[\left(\bar{\alpha}^2 \Pi_3 + \frac{U'}{U} \Pi_3'\right) - \frac{\mathrm{i}\bar{\alpha}}{\cos\theta} \left(U_{\mathrm{c}} \cos\theta \frac{\mathrm{d}A^{\dagger}}{\mathrm{d}\bar{x}_1} - \mathrm{i}S_1 A^{\dagger}\right) \left(\frac{\Pi_1}{U} + \frac{2F_1}{T_0}\right)\right.$$
$$\left. - \mathrm{i}2\bar{\alpha} \frac{\mathrm{d}A^{\dagger}}{\mathrm{d}\bar{x}_1} \left(\Pi_1 + \frac{U}{T_0} F_1\right)\right] \tag{2.32}$$

and so forth, where

$$\mathrm{L} \equiv \frac{1}{T_0} \frac{\mathrm{d}}{\mathrm{d}y} T_0 \frac{\mathrm{d}}{\mathrm{d}y} - \frac{2U'}{U} \frac{\mathrm{d}}{\mathrm{d}y} - \bar{\alpha}^2 \left(1 - \frac{U^2 M^2}{T_0} \cos^2\theta\right) \tag{2.33}$$

is the linear compressible Rayleigh operator.

Equations (2.29) and (2.30) must, in general, be solved numerically. Fortunately, it turns out that it is only necessary to know the local behaviour of their solutions at the critical layer where $U(y) = 0$. We shall use the subscript c to denote quantities at the critical level. Figures 20 and 21 of Jackson & Grosch (1988) show that the mode with the largest maximum spatial growth rate (over all frequencies) is an oblique wave. Their figure 5 shows that the neutral phase velocity of this mode is subsonic relative to both streams when M is less than five, and therefore, according to Lees & Lin (1946), has a critical level at one of the generalized inflection points, where $(U'/T_0)' = 0$ or

$$\frac{U_{\mathrm{c}}''}{U_{\mathrm{c}}'} = \frac{T_{\mathrm{c}}'}{T_{\mathrm{c}}}. \tag{2.34}$$

This remains true for Mach numbers up to about seven. Since real gas effects probably become important at higher Mach numbers, we restrict the analysis to this case and suppose that the critical level is at a generalized inflection point.

This, so called, 'non-singular' critical level, which we can always suppose to lie at the origin $y = 0$, is then a regular singular point for the operator (2.33), and hence (2.30) possesses two linearly independent homogeneous solutions that are completely non-singular. We denote them by $\tilde{\Pi}^{(1)}$ and $\tilde{\Pi}^{(2)}$, and it follows from general Frobeneous theory (Goldstein & Braun 1973, pp. 176–187) that we can choose them so that

$$\tilde{\Pi}^{(1)} = 1 - \tfrac{1}{2}\bar{\alpha}^2 y^2 + a_4 y^4 + \ldots \tag{2.35}$$

and

$$\tilde{\Pi}^{(2)} = y^3 + \ldots \tag{2.36}$$

as $y \to 0$, where

$$a_4 \equiv \tfrac{1}{4}\bar{\alpha}^2\left[\frac{T_c''}{T_c} - \frac{2}{3}\frac{U_c'''}{U_c'} - \frac{1}{2}\left(\frac{U_c''}{U_c'}\right)^2 - \tfrac{1}{2}\bar{\alpha}^2 - \frac{M^2 U_c'^2}{T_c}\cos^2\theta\right]. \tag{2.37}$$

Then we can write

$$\Pi_1 = \frac{U_c'}{T_c}\left[\tilde{\Pi}^{(1)} + \tfrac{1}{3}\bar{\alpha}^2\left(b_1 + \frac{1}{2}\frac{U_c''}{U_c'}\right)\tilde{\Pi}^{(2)}\right], \tag{2.38}$$

where b_1 is a constant, which must be determined along with $\bar{\alpha}$ by solving (2.29) numerically and imposing proper boundary conditions at infinity (Gropengeisser 1969). It now follows from (2.31) that

$$F_1 = -\left(\frac{T_c''}{T_c} - \frac{U_c'''}{U_c'} - \bar{\alpha}^2 - \frac{M^2 U_c'^2}{T_c}\cos^2\theta\right)y - b_1\left(1 + \frac{U_c''}{U_c'}y\right) + \ldots \quad \text{as} \quad y \to 0 \tag{2.39}$$

and similarly from appropriate equations obtained from (2.22) and (2.23) that

$$\Phi_1 = 1 - b_1 y + \ldots \tag{2.40}$$

and (see Reshotko 1960)

$$\Theta_1 = T_c'/(U_c' \cos\theta y) + \ldots \quad \text{as} \quad y \to 0. \tag{2.41}$$

It follows from (2.33), (2.35), and (2.36) that there exists two continuous functions, say $\Pi_{P,1}$ and $\Pi_{P,2}$, which satisfy

$$\mathrm{L}\Pi_{P,1} = \frac{T_c}{U_c'}\left[\frac{U'}{U^2}\frac{\mathrm{d}}{\mathrm{d}y} + \frac{U}{T_0}(M\bar{\alpha}\cos\theta)^2\right]\Pi_1, \tag{2.42}$$

and

$$\mathrm{L}\Pi_{P,2} = T_c\left[1 - \frac{(MU)^2\cos^2\theta}{T_0}\right]\Pi_1/U_c', \tag{2.43}$$

but are, in general, unbounded at $y = \pm\infty$. $\Pi_{P,1}$ will behave like

$$\tilde{e}_1 + \tilde{e}_2 y + \tilde{e}_3 y^2 + \tilde{e}_4 y^3 \ln|y| + \tilde{e}_5 y^3 \quad \text{as} \quad y \to 0$$

and $\Pi_{P,2}$ will be regular there. The relevant solution to (2.30) must then be of the form

$$\Pi_3 = \frac{2\mathrm{i}U_c'}{T_c\bar{\alpha}\cos\theta}\left(U_c\cos\theta\frac{\mathrm{d}A^\dagger}{\mathrm{d}\bar{x}_1} - \mathrm{i}S_1 A^\dagger\right)\left[\Pi_{P,1} + c_{2,1}^{\pm}\tilde{\Pi}^{(1)} + \tfrac{1}{3}\bar{\alpha}^2\left(b_{2,1}^{\pm} + \frac{1}{2}\frac{U_c''}{U_c'}\right)\tilde{\Pi}^{(2)}\right]$$
$$-2\mathrm{i}\bar{\alpha}\frac{U_c'}{T_c}\frac{\mathrm{d}A^\dagger}{\mathrm{d}\bar{x}_1}\left[\Pi_{P,2} + c_{2,2}^{\pm}\tilde{\Pi}^{(1)} + \tfrac{1}{3}\bar{\alpha}^2\left(b_{2,2}^{\pm} + \frac{1}{2}\frac{U_c''}{U_c'}\right)\tilde{\Pi}^{(2)}\right] \quad \text{for} \quad y \gtrless 0, \tag{2.44}$$

where $b_{2,n}^{\pm}, c_{2,n}^{\pm}$ are real constants (even on the slow scale $\bar{x}_1$), which can only be determined numerically. It can be shown that $c_{2,n}^{+} = c_{2,n}^{-}$ because the critical layer cannot support an $O(\epsilon^{\frac{7}{3}})$ pressure discontinuity (see the streamwise critical-layer momentum equation below).

It now follows from (2.32) that

$$F_3 = e_1(\bar{x}_1) + e_2(\bar{x}_1)\ln|y| + 2\mathrm{i}\bar{\alpha}\frac{\mathrm{d}A^\dagger}{\mathrm{d}\bar{x}_1}b_{2,2}^{\pm}$$
$$-\frac{\mathrm{i}2}{\bar{\alpha}\cos\theta}\left(U_c\cos\theta\frac{\mathrm{d}A^\dagger}{\mathrm{d}\bar{x}_1} - \mathrm{i}S_1 A^\dagger\right)b_{2,1}^{\pm} + \ldots \quad \text{as} \quad y \to \pm 0. \tag{2.45}$$

3. The critical layer

Equation (2.41) clearly shows that the outer expansion (2.14)–(2.18) becomes singular at the critical level. The equations therefore have to be rescaled in this region in order to obtain the so-called critical layer solution. The thickness of the linear, small-growth-rate critical layer is of the same order as the growth rate, i.e. $O(\epsilon^{\frac{2}{5}})$ in the present case. The appropriate scaled transverse coordinate in this region is therefore

$$Y = y/\epsilon^{\frac{2}{5}}. \tag{3.1}$$

Introducing this along with (2.19), (2.28), (2.38)–(2.41), and (2.45) into (2.14)–(2.18) and re-expanding the result shows that

$$\begin{aligned}\bar{u} = {} & \epsilon^{\frac{3}{5}}U_c' \cos\theta Y + \tfrac{1}{2}\epsilon^{\frac{4}{5}}U_c'' \cos\theta Y^2 - \epsilon \operatorname{Re} b_1 A^+ e^{i\bar{\alpha}\zeta} \\ & + \epsilon^{\frac{6}{5}}(\tfrac{1}{3!}U_c''' Y^3 \cos\theta + \text{bounded, } Y\text{-independent terms}) \\ & + \epsilon^{\frac{7}{5}} \ln \epsilon^{\frac{2}{5}} \operatorname{Re} e_2(\bar{x}_1) A^+ e^{i\bar{\alpha}\zeta} + \epsilon^{\frac{7}{5}} \\ & \times \left\{ \operatorname{Re}\left[\left(\frac{U_c'''}{U_c'} - \frac{T_c''}{T_c} + \bar{\alpha}^2 + \frac{M^2 U_c'^2}{T_c} \cos^2\theta - b_1 \frac{U_c''}{U_c'} \right) Y A^+ + e_1 + e_2 \ln|Y| \right.\right. \\ & \left.\left. + 2i\bar{\alpha} \frac{dA^+}{d\bar{x}_1} b^{\pm}_{2,2} - \frac{i2}{\bar{\alpha}\cos\theta}\left(U_c \cos\theta \frac{dA^+}{d\bar{x}_1} - iS_1 A^+ \right) b^{\pm}_{2,1} \right] e^{i\bar{\alpha}\zeta} + \text{harmonics} + \ldots \right\}, \end{aligned} \tag{3.2}$$

$$p = 1 + \epsilon k M^2 \cos\theta \frac{U_c'}{T_c} \operatorname{Re} A^+ e^{i\bar{\alpha}\zeta} + \epsilon^{\frac{6}{5}}(\text{bounded } Y\text{-independent terms}) + \ldots, \tag{3.3}$$

$$T = T_c + \epsilon^{\frac{2}{5}} T_c' Y + \epsilon^{\frac{3}{5}} \frac{T_c'}{U_c' \cos\theta} \frac{1}{Y} \operatorname{Re} A^+ e^{i\bar{\alpha}\zeta} + \epsilon^{\frac{4}{5}} \tfrac{1}{2} T_c'' Y^2 + \ldots, \tag{3.4}$$

$$v = -\epsilon\bar{\alpha} \operatorname{Re} iA^+ e^{i\bar{\alpha}\zeta} + \ldots. \tag{3.5}$$

This suggests that the critical-layer solution should expand like

$$\bar{u} = \epsilon^{\frac{2}{5}} U_c' \cos\theta Y + \tfrac{1}{2}\epsilon^{\frac{4}{5}} U_c'' \cos\theta Y^2 + \epsilon\tilde{u}_1 + \epsilon^{\frac{6}{5}}\tilde{u}_2 + \epsilon^{\frac{7}{5}}\tilde{u}_3 + \ldots, \tag{3.6}$$

$$\bar{v} = -\epsilon^{\frac{3}{5}}\bar{\alpha} \operatorname{Re} iA^+ e^{i\bar{\alpha}\zeta} + \epsilon\tilde{v}_1 + \epsilon^{\frac{6}{5}}\tilde{v}_2 + \epsilon^{\frac{7}{5}}\tilde{v}_3 + \ldots, \tag{3.7}$$

$$\bar{w} = -U_c \sin\theta - \epsilon^{\frac{2}{5}} U_c' \sin\theta Y + \epsilon^{\frac{3}{5}}\tilde{w}_0 + \epsilon^{\frac{4}{5}}\tilde{w}_1 + \epsilon^{\frac{6}{5}}\tilde{w}_2 + \ldots, \tag{3.8}$$

$$p = 1 + \epsilon\tilde{p}_1(\zeta, \bar{x}_1) + \epsilon^{\frac{6}{5}}\tilde{p}_2(\zeta, \bar{x}_1) + \epsilon^{\frac{7}{5}}\tilde{p}_3 + \ldots, \tag{3.9}$$

$$T = T_c + \epsilon^{\frac{2}{5}} T_c' Y + \epsilon^{\frac{3}{5}}\tilde{T}_0 + \epsilon^{\frac{4}{5}}\tilde{T}_1 + \epsilon\tilde{T}_2 + \ldots, \tag{3.10}$$

where we assume that the $\ln \epsilon^{\frac{2}{5}}$ terms have been incorporated into $\tilde{u}_3$, etc.

$$\tilde{p}_1 = \cos\theta k M^2 \frac{U_c'}{T_c} \operatorname{Re} A^+ e^{i\bar{\alpha}\zeta} \tag{3.11}$$

and we have put

$$\bar{v} \equiv \epsilon^{-\frac{2}{5}} v. \tag{3.12}$$

The $\tilde{u}_n$, $\tilde{v}_n$, $\tilde{w}_n$, etc. are functions of ζ, Y, and $\bar{x}_1$, only. They are determined by the inviscid momentum, energy and continuity equations which, when expressed in terms of ζ, Y, and $\bar{x}_1$, can be written as

$$\frac{1}{T}\bar{\mathrm{D}}\bar{\boldsymbol{u}} = -\frac{1}{kM^2 p}\left\{ p_\zeta + \epsilon^{\frac{2}{5}} p_{\bar{x}_1}, \frac{1}{\epsilon^{\frac{4}{5}}} p_Y, 0 \right\}, \tag{3.13}$$

$$\frac{1}{kp}\bar{\mathrm{D}}p = \frac{1}{(k-1)T}\bar{\mathrm{D}}T = -(\bar{u}_\zeta + \bar{v}_Y + \epsilon^{\frac{2}{5}}\bar{u}_{\bar{x}_1}), \tag{3.14}$$

where we have put

$$\bar{\boldsymbol{u}} \equiv \{\bar{u}, \bar{v}, \bar{w}\}, \tag{3.15}$$

$$\bar{\mathrm{D}} \equiv \left(\bar{u} - \frac{\epsilon^{\frac{2}{5}} S_1}{\bar{\alpha}}\right)\frac{\partial}{\partial \zeta} + \bar{v}\frac{\partial}{\partial Y} + \epsilon^{\frac{2}{5}}(\bar{u} + U_c \cos\theta)\frac{\partial}{\partial \bar{x}_1}, \tag{3.16}$$

and subscripts are used to denote partial derivatives with respect to the indicated variables.

It is also convenient to work with the $\bar{z}$-component vorticity equation, which can be written as

$$\bar{\mathrm{D}}\Omega - \Omega\frac{1}{kp}\bar{\mathrm{D}}p = -\frac{1}{\epsilon^{\frac{2}{5}} k M^2 p}[(T_\zeta + \epsilon^{\frac{2}{5}} T_{\bar{x}_1}) p_Y - T_Y(p_\zeta + \epsilon^{\frac{2}{5}} p_{\bar{x}_1})], \tag{3.17}$$

where

$$\Omega \equiv -\frac{1}{\epsilon^{\frac{3}{5}}}\bar{u}_Y + \epsilon^{\frac{2}{5}}\left(\frac{\partial}{\partial \zeta} + \epsilon^{\frac{2}{5}}\frac{\partial}{\partial \bar{x}_1}\right)\bar{v} \tag{3.18}$$

is the $\bar{z}$-component of the vorticity.

Substituting the expansions (3.6)–(3.10) into these equations and using (2.34) we find

$$\tilde{u}_{n\zeta} + \tilde{v}_{nY} + \delta_{n,3}\,\tilde{u}_{(n-2)\bar{x}_1} = -\frac{\delta_{n,3}}{k}\tilde{\mathscr{L}}\tilde{p}_1 \quad \text{for} \quad n = 1, 2, 3, \tag{3.19}$$

$$\tilde{\mathscr{L}}\tilde{T}_0 = T_c' \bar{\alpha}\,\mathrm{Re}\,\mathrm{i}A^\dagger \mathrm{e}^{\mathrm{i}\bar{\alpha}\zeta}, \tag{3.20}$$

$$\tilde{\mathscr{L}}\tilde{T}_1 = \tilde{T}_{0Y}\bar{\alpha}\,\mathrm{Re}\,\mathrm{i}A^\dagger \mathrm{e}^{\mathrm{i}\bar{\alpha}\zeta}, \tag{3.21}$$

$$\tilde{\mathscr{L}}\tilde{Q}_1 = 0, \tag{3.22}$$

$$\tilde{\mathscr{L}}\tilde{Q}_2 = \left[\tilde{Q}_{1Y} - 2\frac{U_c'}{T_c}\cos\theta\tilde{T}_{0Y}\right]\bar{\alpha}\,\mathrm{Re}\,\mathrm{i}A^\dagger \mathrm{e}^{\mathrm{i}\bar{\alpha}\zeta}, \tag{3.23}$$

$$\tilde{\mathscr{L}}\tilde{Q}_3 = \tilde{Q}_{2Y}\bar{\alpha}\,\mathrm{Re}\,\mathrm{i}A^\dagger \mathrm{e}^{\mathrm{i}\bar{\alpha}\zeta} - \left(\frac{U_c'''}{U_c'} - \frac{T_c''}{T_c}\right)\mathrm{Re}\,(U_c \cos\theta A^\dagger_{\bar{x}_1} - \mathrm{i}S_1 A^\dagger)\,\mathrm{e}^{\mathrm{i}\bar{\alpha}\zeta} + \cos\theta\left(\tfrac{1}{2}U_c'' Y^2\frac{\partial}{\partial \zeta} + U_c' Y\frac{\partial}{\partial \bar{x}_1}\right)\tilde{Q}_1, \tag{3.24}$$

where we have put

$$\tilde{\mathscr{L}} \equiv U_c \cos\theta\frac{\partial}{\partial \bar{x}_1} + \left(U_c' \cos\theta Y - \frac{S_1}{\bar{\alpha}}\right)\frac{\partial}{\partial \zeta}, \tag{3.25}$$

$$\tilde{Q}_1 = \tilde{u}_{1Y}, \tag{3.26}$$

$$\tilde{Q}_2 = \tilde{u}_{2Y} - \frac{U_c'}{T_c}\cos\theta\tilde{T}_1 - \tfrac{1}{2}U_c'\left(\frac{U_c'''}{U_c'} - \frac{T_c''}{T_c}\right)\cos\theta Y^2, \tag{3.27}$$

$$\tilde{Q}_3 = \tilde{u}_{3Y} - \bar{\alpha}^2\,\mathrm{Re}\,A^\dagger \mathrm{e}^{\mathrm{i}\bar{\alpha}\zeta} - \frac{T_c'}{T_c}\tilde{u}_1 - U_c' \cos\theta\frac{\tilde{p}_1}{k} - \left(\frac{U_c'''}{U_c'} - \frac{T_c''}{T_c}\right)\mathrm{Re}\,A^\dagger \mathrm{e}^{\mathrm{i}\bar{\alpha}\zeta}, \tag{3.28}$$

and used (3.21) to obtain (3.23) and (3.24) from the $\bar{z}$-vorticity equation (3.17). Comparing these with the inner expansions (3.2)–(3.5) of the outer solution shows that

$$\tilde{T}_0 \to 0, \tag{3.29}$$

and

$$\tilde{Q}_n \to 0 \quad \text{for} \quad n = 1, 2, 3 \quad \text{as} \quad Y \to \pm\infty. \tag{3.30}$$

In fact the entire inner solution will match onto the inner expansions of the outer solution (3.2)–(3.5) (to the order of approximation of the analysis) if

$$\mathrm{Re}\left[2\mathrm{i}\bar{\alpha}A^{\dagger}_{\bar{x}_1}(b^{+}_{2,2}-b^{-}_{2,2})-\frac{\mathrm{i}2}{\bar{\alpha}\cos\theta}(U_{\mathrm{c}}\cos\theta A^{\dagger}_{\bar{x}_1}-\mathrm{i}S_1A^{\dagger})(b^{+}_{2,1}-b^{-}_{2,1})\right]\mathrm{e}^{\mathrm{i}\bar{\alpha}\zeta}$$
$$=\int_{-\infty}^{\infty}\tilde{Q}_3\,\mathrm{d}Y+\text{zeroth and higher harmonics in }\mathrm{e}^{\mathrm{i}\bar{\alpha}\zeta}. \quad (3.31)$$

This equation ultimately determines the outer instability amplitude $A^{\dagger}$ and consequently the growth rate of that wave, but it is first necessary to determine $\tilde{Q}_3$ from (3.19)–(3.24), which can easily be done seriatim, since $\tilde{\mathscr{L}}$ is a simple linear operator (Stewartson 1978, 1981).

The relevant solution to (3.22) is the trivial solution

$$\tilde{Q}_1\equiv 0. \quad (3.32)$$

It is convenient to work in terms of the following normalized variables:

$$\bar{x}=-\tfrac{1}{2}S_1U_{\mathrm{c}}'\bar{x}_1-\bar{x}_0, \quad (3.33)$$

$$\eta=-2\bar{\alpha}\left(Y-\frac{S_1}{\bar{\alpha}U_{\mathrm{c}}'\cos\theta}\right)\Big/S_1U_{\mathrm{c}}, \quad (3.34)$$

$$X=\bar{\alpha}\zeta-X_0, \quad (3.35)$$

$$A=4\bar{\alpha}^2A^{\dagger}\mathrm{e}^{\mathrm{i}X_0}/(U_{\mathrm{c}}S_1)^2U_{\mathrm{c}}', \quad (3.36)$$

$$Q^{(n)}=\cos\theta\bar{\alpha}^2\tilde{Q}_n/S_1^2U_{\mathrm{c}}U_{\mathrm{c}}', \quad (3.37)$$

where the coordinate origin shifts $\bar{x}_0$ and X_0 are chosen so that

$$A\sim\mathrm{e}^{\bar{\kappa}\bar{x}+\mathrm{i}\varphi_0}\quad\text{as}\quad\bar{x}\to-\infty \quad (3.38)$$

(see (2.20)), and the real constant φ_0 represents an, as yet, unspecified, initial phase factor.

It is clear from (3.20)–(3.24) that $\tilde{T}^{(0)}$, $Q^{(2)}$ and $Q^{(3)}$ are functions of the form

$$\tilde{T}_0=\mathrm{Re}\,T_1^{(0)}(\bar{x},\eta)\,\mathrm{e}^{\mathrm{i}X}, \quad (3.39)$$

$$Q^{(2)}=\mathrm{Re}\,[Q_0^{(2)}(\bar{x},\eta)+Q_2^{(2)}(\bar{x},\eta)\,\mathrm{e}^{2\mathrm{i}X}], \quad (3.40)$$

$$Q^{(3)}=\mathrm{Re}\,[Q_1^{(3)}(\bar{x},\eta)\,\mathrm{e}^{\mathrm{i}X}+Q_3^{(3)}(\bar{x},\eta)\,\mathrm{e}^{3\mathrm{i}X}]. \quad (3.41)$$

Our interest here is primarily in the first harmonic, $Q_1^{(3)}$ of $Q^{(3)}$ since it will ultimately determine the amplitude A when $Q^{(3)}$ is substituted into (3.31). Substituting these into (3.19)–(3.34) and integrating the equations sequentially between $-\infty$ and $\bar{x}$, we find that (Stewartson 1978, 1981)

$$T_1^{(0)}=-\frac{\mathrm{i}T_{\mathrm{c}}'U_{\mathrm{c}}S_1}{2\cos\theta\bar{\alpha}}\int_{-\infty}^{\bar{x}}\mathrm{e}^{-\mathrm{i}\eta(\bar{x}-\tilde{x})}A(\tilde{x})\,\mathrm{d}\tilde{x}, \quad (3.42)$$

and it is shown in the Appendix that the harmonic coefficients $Q_0^{(2)}$, $Q_2^{(2)}$ and $Q_1^{(3)}$ are given by (A 1)–(A 3). Integrating (A 3), we obtain

$$\frac{\mathrm{i}}{\pi}\int_{-\infty}^{\infty}Q_1^{(3)}\,\mathrm{d}\eta=-\frac{\mathrm{i}}{2U_{\mathrm{c}}'}\left(\frac{U_{\mathrm{c}}'''}{U_{\mathrm{c}}'}-\frac{T_{\mathrm{c}}''}{T_{\mathrm{c}}}\right)(\tfrac{1}{2}U_{\mathrm{c}}U_{\mathrm{c}}'\cos\theta A_{\bar{x}}+\mathrm{i}A)$$
$$+\frac{\bar{\alpha}T_{\mathrm{c}}'}{2T_{\mathrm{c}}\cos\theta S_1}\int_{-\infty}^{\bar{x}}\int_{-\infty}^{\tilde{x}}A(\tilde{x})\,A(\tilde{\tilde{x}})\,A^*(\tilde{\tilde{x}}+\tilde{x}-\bar{x})\,(\bar{x}-\tilde{x})^2\,\mathrm{d}\tilde{\tilde{x}}\,\mathrm{d}\tilde{x}. \quad (3.43)$$

It is worth noting that the only non-zero contribution to this integral comes from the interaction of the mean flow change with the first harmonic (the last term in (A 3)).

Then substituting (3.43) into (3.31) yields

$$\frac{1}{\bar{\kappa}}A_{\bar{x}} = A - \frac{1}{\gamma}\int_{-\infty}^{\bar{x}}\int_{-\infty}^{\tilde{x}} A(\tilde{x})\,A(\tilde{\tilde{x}})\,A^*(\tilde{\tilde{x}}+\tilde{x}-\bar{x})\,(\bar{x}-\tilde{x})^2\,\mathrm{d}\tilde{\tilde{x}}\,\mathrm{d}\tilde{x}, \tag{3.44}$$

where

$$\gamma \equiv \frac{T_c S_1 \cos\theta}{\bar{\alpha} U_c' T_c'}\left[\frac{T_c''}{T_c} - \frac{U_c'''}{U_c'} + \frac{2\mathrm{i}}{\pi}U_c'(b_{2,1}^+ - b_{2,1}^-)\right], \tag{3.45}$$

$$\frac{1}{\bar{\kappa}} \equiv \left[\frac{S_1 T_c}{\gamma T_c'}\frac{\bar{\alpha}\cos\theta}{\pi}(b_{2,2}^+ - b_{2,2}^-) + \tfrac{1}{2}\mathrm{i}U_c\right]U_c'\cos\theta \tag{3.46}$$

are complex constants.

Equation (3.44) is the final result. It determines the amplitude of the instability wave.

4. Asymptotic solution of the amplitude equation

The principal result of this paper is given by (3.44) together with the upstream boundary condition (3.49). The numerical solutions to this problem, which are discussed in §6, appear to develop a singularity at a finite value of $\bar{x}$, say $\bar{x}_s$. In this section we determine the asymptotic form of those solutions as $\bar{x}\to\bar{x}_s$. To this end we substitute

$$A = \frac{a}{(\bar{x}_s-\bar{x})^{(\frac{5}{2}+\mathrm{i}\sigma)}}, \tag{4.1}$$

where $\bar{x}_s$ and σ are real constants and a is a complex constant, into the integral of (3.44) and change the integration variables from $\tilde{\tilde{x}}$ and $\tilde{x}$ to $(\bar{x}_s-\tilde{\tilde{x}})/(\bar{x}_s-\bar{x})$ and $(\bar{x}_s-\tilde{x})/(\bar{x}_s-\bar{x})$ to show that

$$\int_{-\infty}^{\bar{x}}\int_{-\infty}^{\tilde{x}} A(\tilde{x})\,A(\tilde{\tilde{x}})\,A^*(\tilde{\tilde{x}}+\tilde{x}-\bar{x})\,(\bar{x}-\tilde{x})^2\,\mathrm{d}\tilde{\tilde{x}}\,\mathrm{d}\tilde{x} = \frac{a|a|^2}{(\bar{x}_s-\bar{x})^{\frac{7}{2}+\mathrm{i}\sigma}}D(\sigma), \tag{4.2}$$

where

$$D(\sigma) = \int_1^\infty \frac{(v-1)^2}{v^{\frac{5}{2}+\mathrm{i}\sigma}}\int_v^\infty \frac{\mathrm{d}u\,\mathrm{d}v}{u^{\frac{5}{2}+\mathrm{i}\sigma}(u+v-1)^{\frac{5}{2}-\mathrm{i}\sigma}} = \Delta_{\frac{3}{2}}(\sigma) - 3\Delta_{\frac{1}{2}}(\sigma). \tag{4.3}$$

Here

$$\begin{aligned}\Delta_r(\sigma) &\equiv \int_1^\infty \frac{1}{v^{\frac{5}{2}+\mathrm{i}\sigma}(1-v)^2}\left\{\frac{1}{r+\mathrm{i}\sigma}\left[\left(\frac{2v-1}{v}\right)^{r+\mathrm{i}\sigma}-1\right] - \frac{1}{-r+\mathrm{i}\sigma}\left[\left(\frac{2v-1}{v}\right)^{-r+\mathrm{i}\sigma}-1\right]\right\}\mathrm{d}v \\ &= \sum_{n=1}^{\infty}\frac{(-1)^n}{n(n+1)(\frac{7}{2}+\mathrm{i}\sigma)_n}[(1-r-\mathrm{i}\sigma)_n - (1+r-\mathrm{i}\sigma)_n],\end{aligned} \tag{4.4}$$

where $(\alpha)_n$ denotes the generalized factorial function $\Gamma(\alpha+n)/\Gamma(\alpha)$ in the usual notation.

$A_{\bar{x}}$ becomes large compared with A as $\bar{x}\to\bar{x}_s$, and the left-hand side of (3.44) is balanced by the integral term on the right-hand side. Substituting (4.1) into the left-hand side shows that the two terms will balance when σ satisfies

$$\frac{D(\sigma)}{\frac{5}{2}+\mathrm{i}\sigma} = \frac{-\gamma}{|a|^2\bar{\kappa}}. \tag{4.5}$$

Figure 1 shows σ as a function of $\arg(\gamma/\bar{\kappa}) = \arg[D/(\frac{5}{2}+\mathrm{i}\sigma)]$. Figure 2 is a plot of $|\gamma|\,|a|^2/|\bar{\kappa}| = |D/(\frac{5}{2}+\mathrm{i}\sigma)|$ as a function of $\arg(\gamma/\bar{\kappa})$.

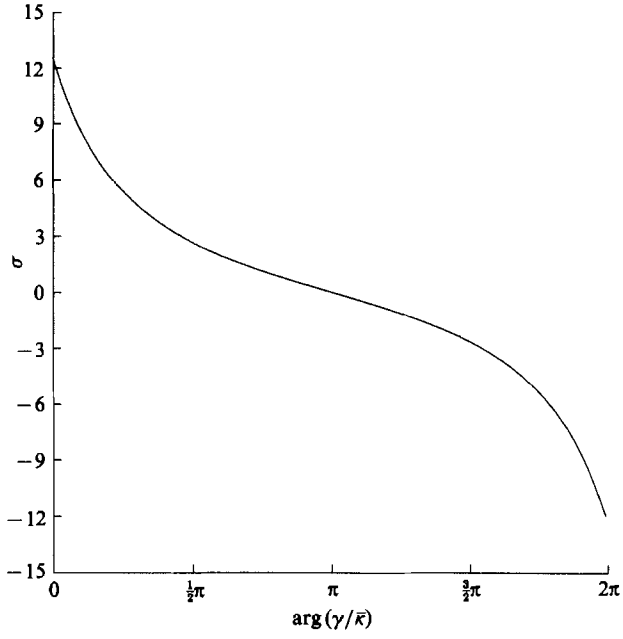

FIGURE 1. σ *vs.* $\arg(\gamma/\bar{\kappa})$.

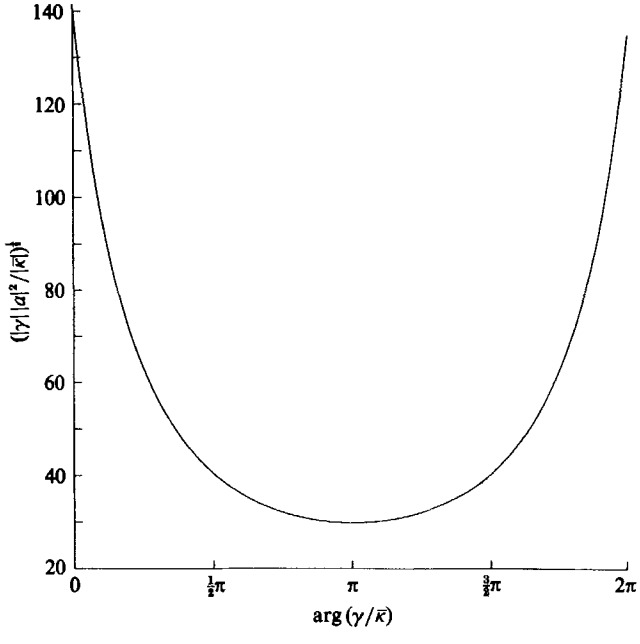

FIGURE 2. $|\gamma||a|^2/|\bar{\kappa}|$ *vs.* $\arg(\gamma/\bar{\kappa})$.

5. The viscous solution

The preceding analysis is easily extended to the viscous case where the scaled viscous parameter

$$\lambda = 1/Re\, e^{\frac{6}{5}} \tag{5.1}$$

and the Prandtl number σ_0 are both of order one. The flow outside the critical layer

is only slightly affected by viscosity and matching with the altered solution requires that we replace the coefficient of $\epsilon^{\frac{4}{5}}$ in (3.6) by $\frac{1}{2}U_c''(\cos\theta Y^2 + 4\lambda_c \cos^2\theta\,\bar{x}_1/U_c)$, and allow $\tilde{u}_2$ and $\tilde{w}_2$ to depend on $\bar{z}$ through the additional terms $-2\lambda_c U_c'' \sin\theta\cos\theta\,\bar{z}/U_c$ and $-2\lambda_c U_c'' \sin^2\theta\,\bar{z}/U_c$, where

$$\lambda_c \equiv \lambda\mu(T_c)\,T_c$$

and $\mu = \mu(T)$ is the normalized viscosity.

The additional term

$$\frac{\lambda\epsilon^{\frac{2}{5}}}{p}\frac{\partial}{\partial Y}\mu\bar{u}_Y$$

will appear on the right-hand side of (3.13), the second member of (3.14) will be replaced by

$$\frac{1}{k-1}\left[\frac{1}{T}\bar{D}T - \frac{\lambda\epsilon^{\frac{2}{5}}}{p}\frac{\partial}{\partial Y}\frac{\mu T_Y}{\sigma_0} - \frac{\lambda\epsilon^{\frac{2}{5}}}{p}(k-1)M^2\mu(\bar{u}_Y^2 + \bar{w}_Y^2)\right],$$

the operator (3.16) has the additional term $\bar{w}\partial/\partial\bar{z}$, and the terms

$$\frac{\lambda\epsilon^{\frac{2}{5}}\Omega}{p}\left[M^2(k-1)\,\mu(\bar{u}_Y^2 + \bar{w}_Y^2) + \frac{\partial}{\partial Y}\left(\frac{\mu}{\sigma_0}T_Y\right)\right]$$

$$-\frac{\lambda\epsilon^{\frac{2}{5}}T}{p}\frac{\partial^2}{\partial Y^2}\mu\Omega - \lambda\epsilon^{\frac{2}{5}}\left[\frac{\partial}{\partial Y}\left(\frac{T}{p}\right)\right]\frac{\partial}{\partial Y}\mu\Omega - \Omega\bar{w}_{\bar{z}} + \frac{1}{\epsilon^{\frac{2}{5}}}\bar{w}_Y\,\bar{u}_{\bar{z}}$$

will appear on the left-hand side of (3.17) to the required order of approximation.

For simplicity we suppose that the viscosity $\mu(T)$ is given by Chapman's law

$$\mu(T) = CT,$$

where C is Chapman's constant, and consider only the case where

$$\sigma_0 \equiv 1. \tag{5.2}$$

The analysis then proceeds as in §3 but the differential operator in (3.20)–(3.24) must be replaced by

$$\tilde{\mathscr{L}} - \lambda_c\frac{\partial^2}{\partial Y^2},$$

the additional terms

$$\frac{\lambda_c}{T_c}[U_c''\cos\theta\tilde{T}_{0Y} + 2(M^2(k-1)\,U_c'^2 - T_c\,U_c''/U_c)\cos\theta\sin\theta\tilde{w}_{0Y}]$$

appear on the right-hand side of (3.24) (after making use of the fact that (3.32) still holds), $\tilde{Q}_2$ is now defined by (3.28) plus

$$\frac{\lambda_c\bar{x}_1}{T_c}\left[\frac{3T_c'\,U_c''}{U_c} - U_c'\,M^2(k-1)\right] - \frac{\lambda_c\,U_c'}{U_c}\left(\frac{U_c'''}{U_c'} - \frac{T_c''}{T_c}\right)\bar{x}_1,$$

and $\tilde{T}_1$ is replaced by

$$\tilde{T}_1 + \frac{\lambda_c\bar{x}_1}{U_c\cos\theta}\left[M^2(k-1)\,U_c'^2 + \frac{T_c'^2}{T_c}\right].$$

These equations, along with the corresponding equation for $\tilde{w}_0$ are easily solved seriatim using the Fourier transform method of Hickernell (1984). Upon introducing the Fourier transform pair

$$\hat{F}(k) = \int_{-\infty}^{\infty} e^{-ik\eta}F(\eta)\,d\eta, \quad F(\eta) = \frac{1}{2\pi}\int_{-\infty}^{\infty} e^{ik\eta}\hat{F}(k)\,dk, \tag{5.3}$$

(3.42) and (A 1) become

$$\hat{T}_1^{(0)} = -\frac{\mathrm{i}\pi T_c' U_c S_1}{\bar{\alpha}\cos\theta} A(\bar{x}+k)\, H(-k)\, \mathrm{e}^{\bar{\lambda}k^3/3} \tag{5.4}$$

and

$$\hat{Q}_0^{(2)} = \frac{\mathrm{i}\pi\bar{\alpha}T_c'}{T_c S_1} kH(-k)\, \mathrm{e}^{\bar{\lambda}k^3/3} \int_{-\infty}^{\bar{x}} \mathrm{e}^{-\bar{\lambda}k^2(\bar{x}-\tilde{x})} A(\tilde{x}+k)\, A^*(\tilde{x})\, \mathrm{d}\tilde{x} \tag{5.5}$$

respectively, where $H(k)$ is the Heaviside function $H(k) = 1, 0$ for $k \gtrless 0$ and

$$\bar{\lambda} \equiv \frac{8\lambda_c \bar{\alpha}^2}{(-S_1 U_c)^3 U_c' \cos\theta} \tag{5.6}$$

is a new scaled viscous parameter and $\hat{Q}_1^{(3)}$ is given by a similar formula.

Using this new solution in (3.31) shows that the final equation (3.44) now generalizes to

$$\frac{1}{\bar{\kappa}}\frac{\mathrm{d}A}{\mathrm{d}\bar{x}} = A - \frac{1}{\gamma}\int_{-\infty}^{\bar{x}}\int_{-\infty}^{\tilde{x}} \mathrm{e}^{-\bar{\lambda}(\bar{x}-\tilde{x})^2[3(\bar{x}-\tilde{\tilde{x}})-(\bar{x}-\tilde{x})]/3} \times A(\tilde{x})\, A(\tilde{\tilde{x}})\, A^*(\tilde{\tilde{x}}+\tilde{x}-\bar{x})\, (\bar{x}-\tilde{x})^2\, \mathrm{d}\tilde{\tilde{x}}\, \mathrm{d}\tilde{x}. \tag{5.7}$$

The only new term in this generalized equation is the exponential factor whose argument is always negative. This term is therefore memory destroying and becomes very small as $\bar{x} \to \infty$ unless $\tilde{\tilde{x}} \approx \tilde{x} \approx \bar{x}$. It follows that

$$\frac{1}{\bar{\kappa}} A_{\bar{x}} \to A - \frac{1}{\gamma \bar{\lambda}^{\frac{4}{3}}} A|A|^2 Q \quad \text{as} \quad \bar{x} \to \infty, \tag{5.8}$$

where

$$Q \equiv \int_0^\infty \mathrm{e}^{-(\frac{2}{3})S^3}\, \mathrm{d}S = \tfrac{1}{2}(\tfrac{2}{3})^{\frac{2}{3}}\Gamma(\tfrac{1}{3}), \tag{5.9}$$

and consequently that

$$|A|^2 \to \frac{\mathrm{Re}\,\bar{\kappa}}{\mathrm{Re}\,\dfrac{\bar{\kappa}}{\gamma}} \frac{\bar{\lambda}^{\frac{4}{3}}}{Q} \tag{5.10}$$

and

$$\mathrm{Im}\frac{A'}{A} \to \left|\frac{\bar{\kappa}}{\gamma}\right|^2 \frac{\mathrm{Im}\,\gamma}{\mathrm{Re}\,\bar{\kappa}/\gamma} \tag{5.11}$$

as $\bar{x} \to \infty$, provided

$$\mathrm{Re}\frac{\bar{\kappa}}{\gamma} > 0. \tag{5.12}$$

Thus, unlike (3.44), the viscous amplitude equation admits an equilibrium solution. Numerical computation must be used to determine whether the solution of (5.7) that matches with the upstream linear solution goes to the asymptotic limit (4.1) or (5.10) in any given case.

6. Numerical results and discussion

The relevant solutions to (3.44) and (3.38) involve the two complex parameters $\bar{\kappa}$ and γ and the still unspecified initial phase factor φ_0. But introducing the rescaled variables $A/|\gamma|^{\frac{1}{3}}|\bar{\kappa}|^2$ and $|\bar{\kappa}|\,\bar{x} - \bar{x}_0$, where $\bar{x}_0$ and φ_0 are chosen so that

$$\frac{\bar{\kappa}}{|\bar{\kappa}|}\bar{x}_0 + \mathrm{i}\varphi_0 = \ln|\gamma|^{\frac{1}{3}}|\bar{\kappa}|^2, \tag{6.1}$$

shows that these solutions can be completely characterized by the two imaginary parameters $\ln(\bar{\kappa}/|\bar{\kappa}|)$ and $\ln(\gamma/|\gamma|)$, or equivalently by the arguments of $\bar{\kappa}$ and γ. The real part of $\bar{\kappa}$ is the scaled growth rate of the upstream linear instability wave in the

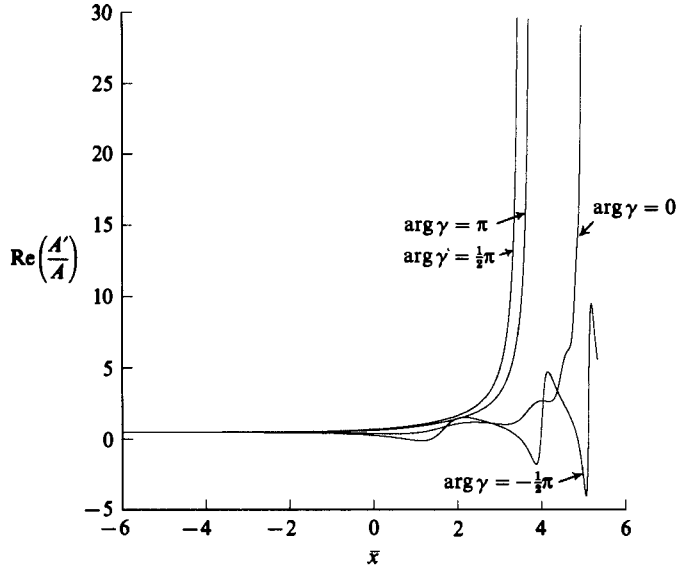

FIGURE 3. $\mathrm{Re}\,A'/A$ *vs.* $\bar{x}$ ($\arg\bar{\kappa} = -\frac{1}{3}\pi$).

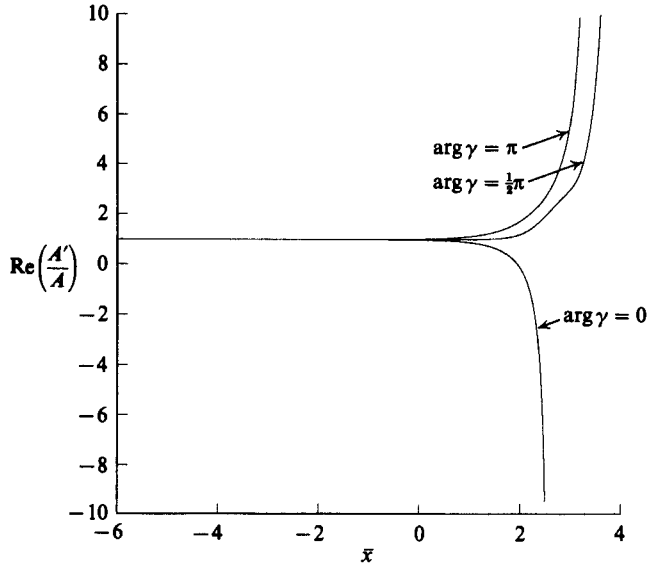

FIGURE 4. $\mathrm{Re}\,A'/A$ *vs.* $\bar{x}$ ($\arg\bar{\kappa} = 0$).

vicinity of its neutral stability point, and the imaginary part is the scaled deviation of the wavenumber from its neutral value corresponding to the prescribed Strouhal-number deviation S_1.

Equation (3.44) was solved numerically by using a fourth-order predictor–corrector scheme to advance the solution downstream from the prescribed upstream linear state (3.38). The double integrals were computed by using the trapezoidal rule with the upstream 'tails' evaluated analytically from the upstream linear solutions. $\bar{\kappa}$ and γ must, in general, be found numerically by solving the homogeneous and inhomogeneous Rayleigh's equations (2.33), (2.42), and (2.43).

Figures 3–5 are plots of the instability wave growth rate $|A|_{\bar{x}}/|A|$ for various values

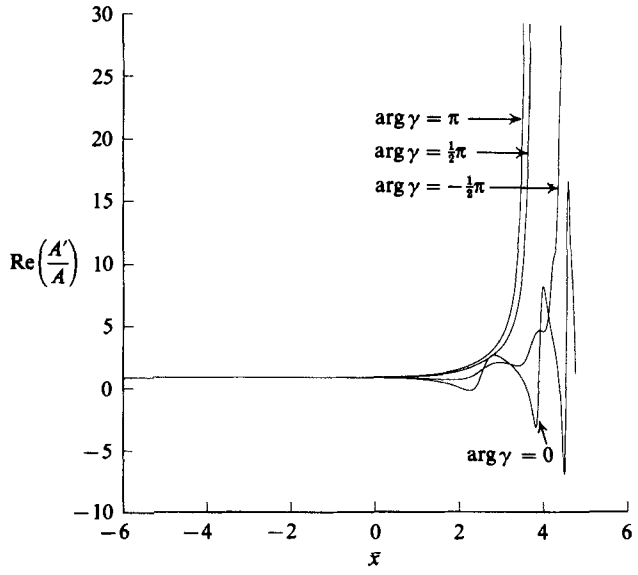

FIGURE 5. $\mathrm{Re}\,A'/A$ *vs.* $\bar{x}$ ($\arg\bar{\kappa} = -\frac{1}{6}\pi$).

of $\arg\gamma$ and $\arg\bar{\kappa}$. We only show results for $-\frac{1}{2}\pi < \arg\bar{\kappa} < 0$ because (3.44) implies that $A(\bar{x}, \bar{\kappa}^*, \gamma^*) = A^*(\bar{x}, \bar{\kappa}, \gamma)$. Considerable care was taken to ensure that the oscillations in figure 5 were not due to the numerics. The reason for this behaviour is given below. Notice that the upstream linear growth rate is initially reduced when $-\frac{1}{2}\pi < \arg(\bar{\kappa}/\gamma) < \frac{1}{2}\pi$. This is because the nonlinear term behaves like $-|A|^2 A/(64\gamma\bar{\kappa}_r^4)$ for small $|A|$, where $\bar{\kappa}_r \equiv \mathrm{Re}\,\bar{\kappa}$. The effective growth rate is therefore reduced by the factor

$$1 - |A|^2 \cos(\arg\bar{\kappa} - \arg\gamma)/(64|\gamma|\,\bar{\kappa}_r^4 \cos(\arg\bar{\kappa})).$$

But (except in the special case† $\arg\gamma = \arg\bar{\kappa} = 0$) this trend is eventually reversed, and the growth rate rapidly increases until the amplitude becomes singular at some finite downstream distance for all values of $\arg(\bar{\kappa}/\gamma)$.

This is shown somewhat better in figures 6–8, which are plots of the real part of $\ln A$ versus the scaled streamwise coordinate $\bar{x}$. Also shown in the figures are the results computed from the asymptotic solution (4.1), with the singularity location $\bar{x}_s$ determined from the numerical solution. The latter solutions clearly approach the asyptotic result as $|\bar{x}_s - \bar{x}|$ becomes small. Since (4.1) implies that the asymptotic growth rate $|A|_{\bar{x}}/|A|$ behaves like $(|A|/|a|)^{\frac{2}{5}}$ in the vicinity of the singularity, the initial scaling, i.e. growth rate $= O(\epsilon^{\frac{2}{5}})$, is unchanged by the singularity. This suggests that the basic asymptotic structure of the critical layer will remain intact, and the present solution will not break down until the amplitude $|A|$ of the external instability wave becomes order one. The flow will then be fully nonlinear and unsteady in the main part of the shear layer, i.e. it will be governed by the full Euler's equations there.

Equations (2.10), (2.14), (2.19), (3.33), (3.45), and (4.1) show that this occurs when

$$x - x_s = O(1), \tag{6.2}$$

where

$$x_s \equiv \frac{\bar{x}_s + \bar{x}_0}{-\frac{1}{2}\epsilon^{\frac{3}{5}} S_1 U_c' \cos\theta} \tag{6.3}$$

† The exceptional case cannot occur for any physically realizable flow and will not be considered further.

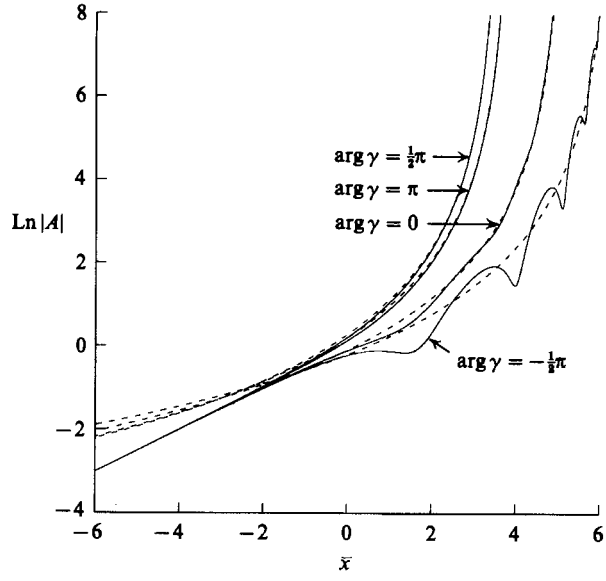

FIGURE 6. $\mathrm{Ln}|A|$ *vs.* $\bar{x}$ ($\arg\bar{\kappa} = -\frac{1}{3}\pi$).

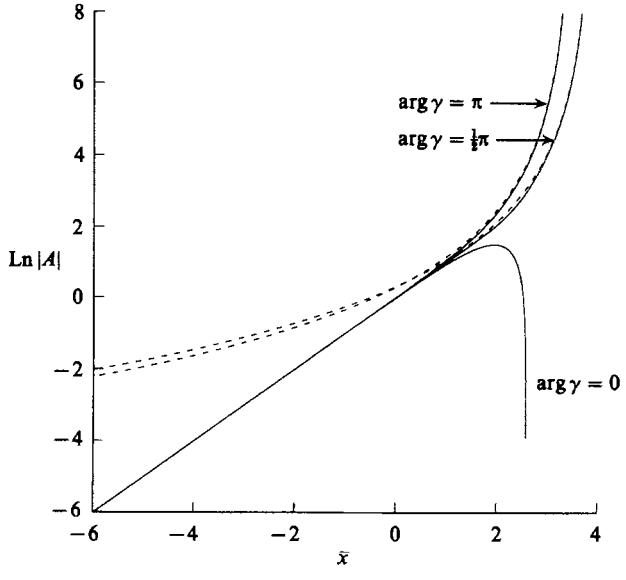

FIGURE 7. $\mathrm{Ln}|A|$ *vs.* $\bar{x}$ ($\arg\bar{\kappa} = 0$).

is the singularity location in the unscaled streamwise coordinates. The fully nonlinear region therefore has a streamwise lengthscale on the order of the shear layer width.

Figures 6–8 show that the instability wave amplitude undergoes successive oscillations upstream of the singularity for certain combinations of $\arg\bar{\kappa}$ and $\arg\gamma$. Similar behaviour was observed in the two dimensional analysis of Goldstein & Leib (1988) and in the calculations of Benney & Maslowe (1975), Huerre (1977), and Miura & Sato (1978). The amplitude oscillations imply periodic reversal of energy transfer between the fluctuations and the mean flow, and possibly between the fluctuations themselves. By considering the Reynolds-stress changes that occur with nutating

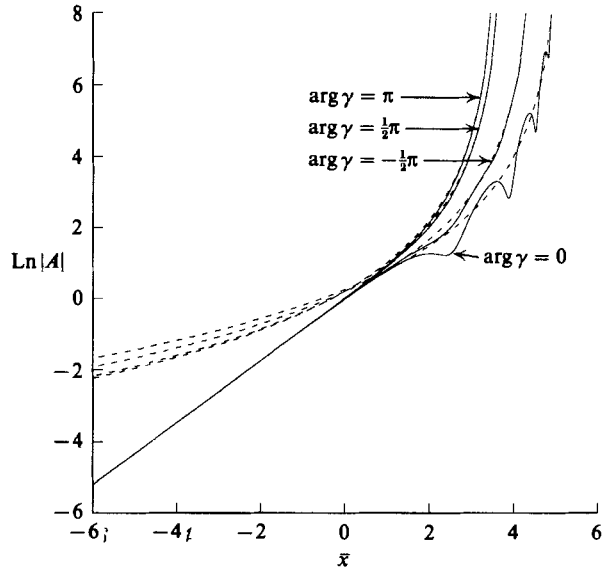

FIGURE 8. $\mathrm{Ln}|A|$ *vs.* $\bar{x}$ ($\arg\bar{\kappa} = -\frac{1}{6}\pi$).

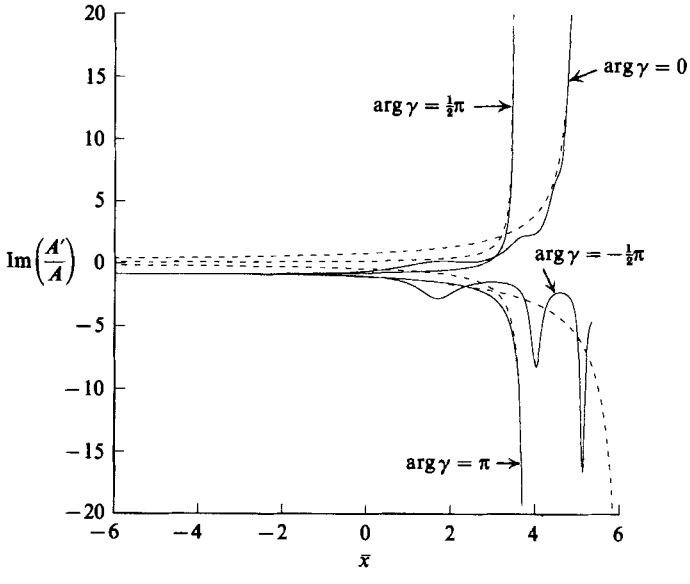

FIGURE 9. $\mathrm{Im}\,A'/A$ *vs.* $\bar{x}$ ($\arg\bar{\kappa} = -\frac{1}{3}\pi$). Dashed lines are asymptotic results computed from (4.1).

elliptic vortices, Browand & Ho (1983) came up with a simple kinematic explanation for this phenomenon. The reader is referred to Ho & Huerre (1984, p. 410) for details.

It is also worth noting that the asymptotic instability wave amplitude is uniquely determined by the asymptotic solution and is therefore independent of the upstream conditions. Figures 9–11 show the wavelength reduction $\mathrm{Im}\,(A_{\bar{x}}/A)$ as a function of the scaled streamwise coordinate $\bar{x}$. The dashed lines are the asymptotic results computed from (4.1).

The numerical scheme used for the inviscid calculations was found to be

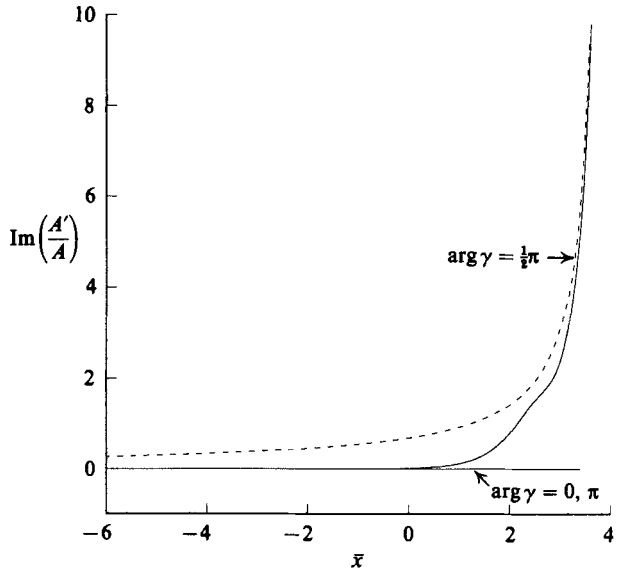

FIGURE 10. $\mathrm{Im}\,A'/A$ *vs.* $\bar{x}$ ($\arg\bar{\kappa} = 0$). Dashed lines are asymptotic results computed from (4.1).

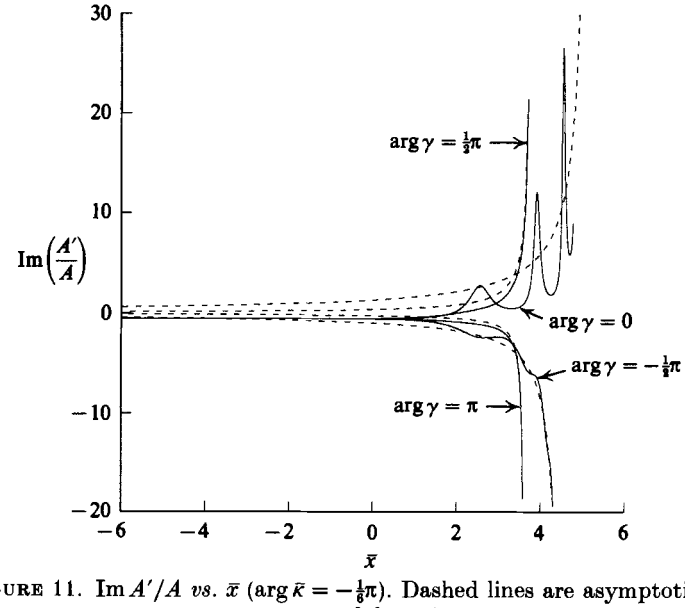

FIGURE 11. $\mathrm{Im}\,A'/A$ *vs.* $\bar{x}$ ($\arg\bar{\kappa} = -\frac{1}{8}\pi$). Dashed lines are asymptotic results computed from (4.1).

inadequate for computing the amplitude function A over the long distances required for certain viscous cases. To compute these cases we introduce

$$\tilde{\eta} = \frac{\bar{x}-\tilde{\bar{x}}}{\bar{x}-\tilde{x}}, \quad \tilde{\zeta} = \bar{\lambda}^{\frac{1}{3}}(\bar{x}-\tilde{x})$$

as new variables of integration in (5.7).

Figure 12 shows numerical solutions of (5.7) for a case when the inequality (5.12) is violated. The effects of increasing the viscous parameter $\bar{\lambda}$ is to keep the growth of the instability wave linear over a longer distance and delay the explosive growth

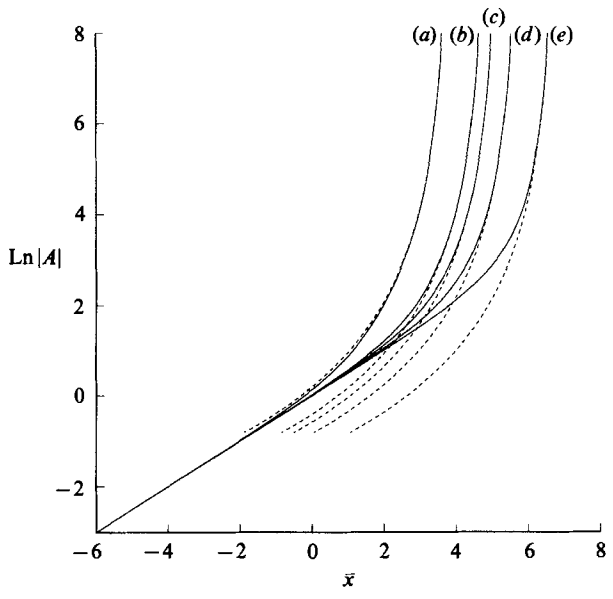

FIGURE 12. $\mathrm{Ln}\,|A|$ *vs.* $\bar{x}$ ($\arg\bar{\kappa} = -\frac{1}{3}\pi$, $\arg\gamma = \pi$, $\bar{\lambda} = 0, 1, 2, 5, 20$, curves (*a–e*) respectively.) Dashed lines are asymptotic results computed from (4.1).

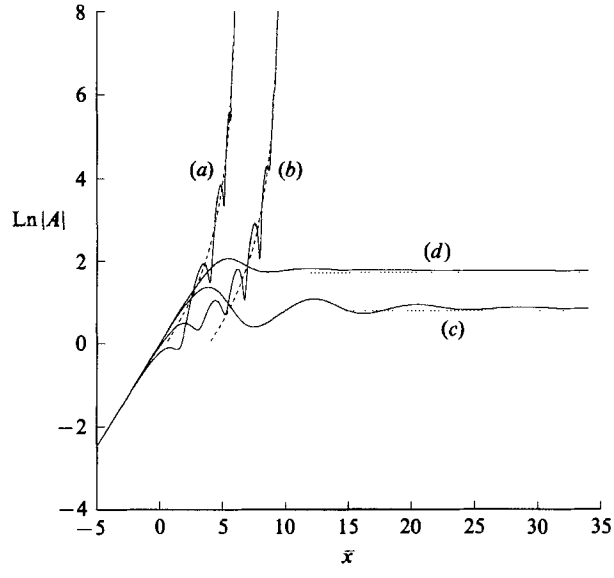

FIGURE 13. $\mathrm{Ln}\,|A|$ *vs.* $\bar{x}$ ($\arg\bar{\kappa} = -\frac{1}{3}\pi$, $\arg\gamma = -\frac{1}{2}\pi$, $\bar{\lambda} = 0, \frac{1}{2}, 5, 20$, curves (*a–d*) respectively.) Dashed lines show asymptotic results computed from (4.1), dotted lines show the finite-amplitude equilibrium given by (5.10).

associated with the singularity. The asymptotic solution in the vicinity of the singularity is still given by (4.1) for this case and is shown as the dashed curves in figure 12. For this choice of $\arg\bar{\kappa}$ and $\arg\gamma$ the singularity can be delayed but not eliminated for any finite value of $\bar{\lambda}$.

In figures 13 and 14 we show the numerical results for two cases when (5.12) is

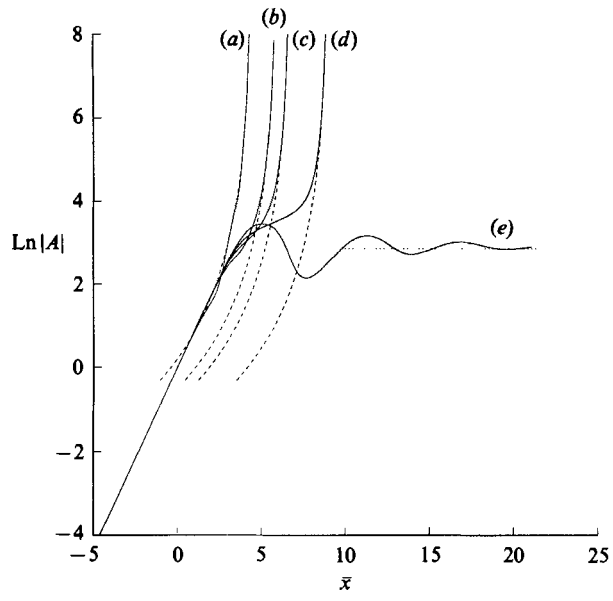

FIGURE 14. Ln$|A|$ *vs.* $\bar{x}$ ($\arg\bar{\kappa} = -\frac{1}{6}\pi$, $\arg\gamma = -\frac{1}{2}\pi$, $\bar{\lambda} = 0, 10, 20, 30, 50$, curves (*a–e*) respectively.) Dashed lines show asymptotic results computed from (4.1), dotted lines show the finite-amplitude equilibrium given by (5.10).

satisfied. For these cases it can be seen that the solution goes to the finite-amplitude equilibrium solution given by (5.10) for sufficiently large $\bar{\lambda}$. The latter are shown dotted on the figures. The minimum value of $\bar{\lambda}$ for which this occurs is a function of $\arg\bar{\kappa}$ and $\arg\gamma$. For smaller values of $\bar{\lambda}$ the solution becomes singular and the asymptotic solution is again given by (4.1) (shown dashed).

The two parameters $\bar{\kappa}$ and γ which appear in the amplitude evolution equations (3.44) and (5.7) involve the constants $b^+_{2,1} - b^-_{2,1}$ and $b^+_{2,2} - b^-_{2,2}$ defined by (2.44). The latter must be determined by numerical solution of the inhomogeneous Rayleigh equations (2.42) and (2.43). This calculation was carried out for a few specific cases and the corresponding values of $\bar{\kappa}$ and γ are presented in figure 15.

The mean velocity profile was taken to be a tanh one in the Howarth (1948) coordinates with the mean temperature given in terms of the velocity by a relation valid for $\sigma_0 = 1$.

Figure 15 shows the real and imaginary parts of $\gamma\bar{\alpha}U_c' T_c'/(T_c S_1 \cos\theta)$ and $\bar{\kappa}U_c' \cos\theta$ for the case when the lower stream is heated to twice the upper stream temperature ($T_2 = 2$), and the angle of propagation of the instability wave is 60° over a range of Mach numbers. At $M = 2.5$ the maximum linear growth rate occurs in the vicinity of this value of θ (Jackson & Grosch 1988, figure 20*a*). In addition the numerically computed values of $\bar{\kappa}$ and γ at this Mach number are within the range (5.12). Therefore we expect that, for this set of physical parameters, the most rapidly growing linear instability wave would eventually saturate and approach an equilibrium condition due to nonlinear critical-layer effects when $\bar{\lambda}$ is sufficiently large.

The authors would like to thank Drs Lennart Hultgren, J. Gajjar, S. J. Cowley, and S. W. Choi for their helpful comments on the manuscript and Dr S. Khandelwal for his help with the numerical calculations.

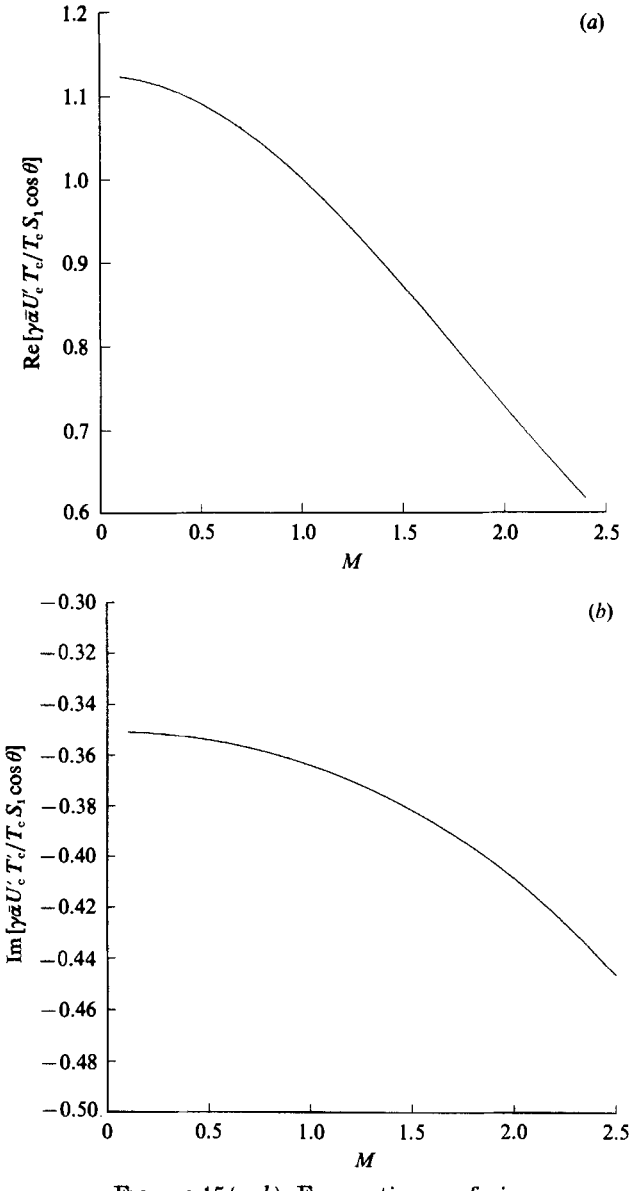

FIGURE 15(*a*, *b*). For caption see facing page.

Appendix

In this Appendix we determine the first-harmonic component $Q_1^{(3)}$ of $Q^{(3)}$. Substituting (3.33), (3.37), (3.39) to (3.41) into (3.23) and integrating, we find that

$$Q_0^{(2)} = -\frac{\mathrm{i}\bar{\alpha}T_c'}{2T_c S_1}\int_{-\infty}^{\bar{x}} A^*(\tilde{x}) \int_{-\infty}^{\tilde{x}} \mathrm{e}^{-\mathrm{i}\eta(\tilde{x}-\tilde{\tilde{x}})}(\tilde{x}-\tilde{\tilde{x}})A(\tilde{\tilde{x}})\,\mathrm{d}\tilde{\tilde{x}}\,\mathrm{d}\tilde{x}, \tag{A 1}$$

where the asterisk denotes complex conjugates and

$$Q_2^{(2)} = -\frac{\bar{\alpha}T_c'}{2\mathrm{i}S_1 T_c}\mathrm{e}^{-2\mathrm{i}\eta\bar{x}}\int_{-\infty}^{\bar{x}} A(\tilde{x})\,\mathrm{e}^{\mathrm{i}\eta\tilde{x}}\int_{-\infty}^{\tilde{x}} \mathrm{e}^{\mathrm{i}\eta\tilde{\tilde{x}}}A(\tilde{\tilde{x}})(\tilde{x}-\tilde{\tilde{x}})\,\mathrm{d}\tilde{\tilde{x}}\,\mathrm{d}\tilde{x}. \tag{A 2}$$

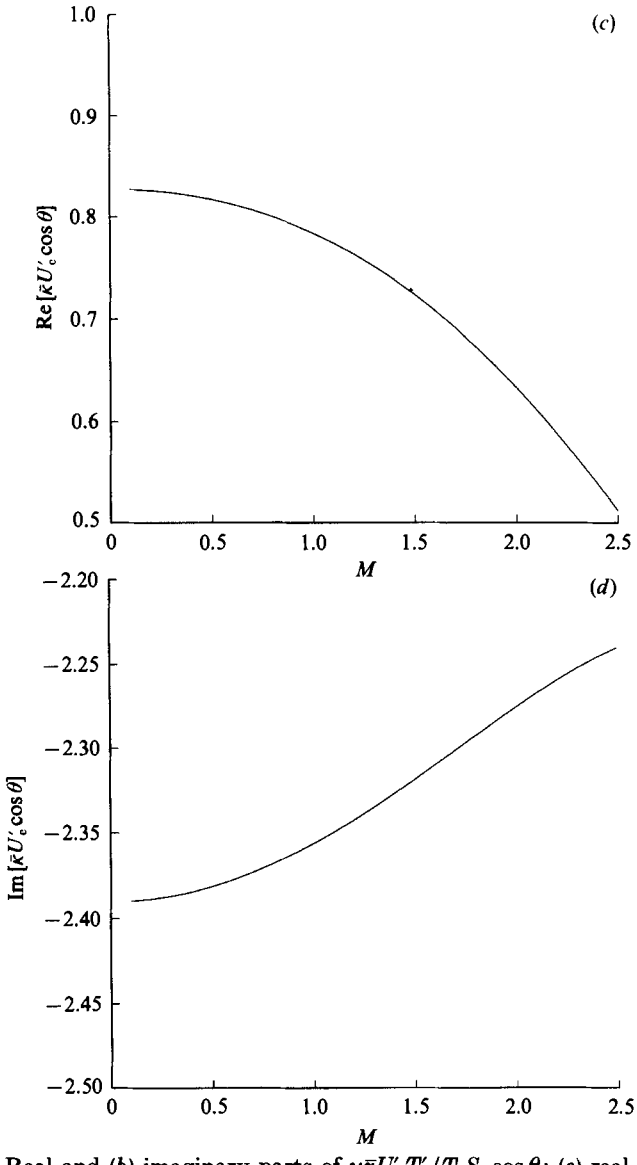

FIGURE 15. (*a*) Real and (*b*) imaginary parts of $\gamma\bar{\alpha}U_c'T_c'/T_cS_1\cos\theta$; (*c*) real and (*d*) imaginary parts of $\bar{\kappa}U_c'\cos\theta$; for $T_2 = 2$, $\theta = 60°$.

Finally, substituting (3.40), and (A 1) and (A 2) into (3.24) and integrating, we obtain

$$
\begin{aligned}
Q_1^{(3)} = &-\frac{1}{2U_c'}\left(\frac{U_c'''}{U_c'}-\frac{T_c''}{T_c}\right)\int_{-\infty}^{\bar{x}} e^{-i\eta(\bar{x}-\tilde{x})}\left[\tfrac{1}{2}U_c'U_c\cos\theta A_{\tilde{x}}+iA(\tilde{x})\right]d\tilde{x}\\
&+\frac{\bar{\alpha}T_c'}{4iT_cS_1\cos\theta}\left\{\int_{-\infty}^{\bar{x}} e^{-i\eta(\bar{x}-\tilde{x})}A^*(\tilde{x})\int_{-\infty}^{\tilde{x}} e^{-2i\eta\tilde{x}}A(\tilde{\tilde{x}})\,e^{i\eta\tilde{\tilde{x}}}\right.\\
&\times\int_{-\infty}^{\tilde{\tilde{x}}} e^{i\eta\tilde{\tilde{\tilde{x}}}}A(\tilde{\tilde{\tilde{x}}})\,(\tilde{\tilde{x}}-\tilde{\tilde{\tilde{x}}})\,(2\tilde{x}-\tilde{\tilde{x}}-\tilde{\tilde{\tilde{x}}})\,d\tilde{\tilde{\tilde{x}}}\,d\tilde{\tilde{x}}\,d\tilde{x}\\
&\left.+2\int_{-\infty}^{\bar{x}} e^{-i\eta(\bar{x}-\tilde{x})}A(\tilde{x})\,\mathrm{Re}\int_{-\infty}^{\tilde{x}} A^*(\tilde{\tilde{x}})\int_{-\infty}^{\tilde{\tilde{x}}} e^{-i\eta(\tilde{\tilde{x}}-\tilde{\tilde{\tilde{x}}})}(\tilde{\tilde{x}}-\tilde{\tilde{\tilde{x}}})^2A(\tilde{\tilde{\tilde{x}}})\,d\tilde{\tilde{\tilde{x}}}\,d\tilde{\tilde{x}}\,d\tilde{x}\right\}.
\end{aligned}
\tag{A 3}
$$

REFERENCES

BENNEY, D. J. & BERGERON, R. F. 1969 A new class of non-linear waves in parallel flows. *Stud. Appl. Maths* **48**, 181–204.

BENNEY, D. J. & MASLOWE, S. A. 1975 The evolution in space and time of nonlinear waves in parallel shear flows. *Stud. Appl. Maths* **54**, 181–205.

BROWAND, F. K. & HO, C. M. 1983 The mixing layer: an example of quasi two-dimensional turbulence. *J. Méc. Theor. Appl.* **2**, 99–102.

CRIGHTON, D. G. & GASTER, M. 1987 Stability of slowly diverging jet flow. *J. Fluid Mech.* **77**, 397–413.

GOLDSTEIN, M. E. & BRAUN, W. H. 1973 Advanced methods for the solution of differential equations. *NASA SP*-316.

GOLDSTEIN, M. E. & HULTGREN, L. S. 1988 Nonlinear spatial evolution of an externally excited instability wave in a free shear layer. *J. Fluid Mech.* **197**, 295–330.

GOLDSTEIN, M. E. & LEIB, S. J. 1988 Nonlinear roll-up of externally excited free shear layers. *J. Fluid Mech.* **191**, 481–515.

GROPENGEISSER, H. 1969 Study of the stability of boundary layers and compressible fluids. *Deutsche Luft- und Raunfahnt Rep.* DLR-FB-69-25, *NASA translations* TT-F-12, 786.

HICKERNELL, F. J. 1984 Time-dependent critical layers in shear flows on the beta-plane. *J. Fluid Mech.* **142**, 431–449.

HO, C. M. & HUERRE, P. 1984 Perturbed free shear layers. *Ann. Rev. Fluid Mech.* **16**, 365–424.

HOWARTH, L. 1948 Concerning the effect of compressibility on laminar boundary layers and their separation. *Proc. Soc. Lond.* A **194**, 16–42.

HUERRE, P. 1977 Nonlinear instability of free shear layers. In *Laminar–Turbulent Transition, AGARD CP*, pp. 224–229.

JACKSON, T. L. & GROSCH, C. E. 1988 Spatial stability of a compressible mixing layer. *NASA CR*-181671.

KUMAR, A., BUSHNELL, D. M. & HUSSAINI, M. Y. 1987 A mixing augmentation technique for hypervelocity scramjets. *AIAA paper* 87-1882.

LEES, L. & LIN, C. C. 1946 Investigation of the stability of the laminar boundary layer in a compressible fluid. *NACA TN*-1115.

MIURA, A. & SATO, T. 1978 Theory of vortex nutation and amplitude oscillation in an inviscid shear instability. *J. Fluid Mech.* **86**, 33–47.

PAPAMOSCHOU, D. & ROSHKO, A. 1986 Observations of supersonic free shear layers. *AIAA*-86-0162.

PAPAMOSCHOU, D. & ROSHKO, A. 1988 The compressible turbulent shear layer: an experimental study. *J. Fluid Mech.* **197**, 453–477.

RESHOTKO, E. 1960 Stability of the compressible laminar boundary layer. *GALCIT Memo* 52. Calif. Inst. of Technology, Pasadena, CA.

STEWARTSON, K. 1978 The evolution of the critical layer of a Rossby wave. *Geophys. Astrophys. Fluid Dyn.* **9**, 185–200.

STEWARTSON, K. 1981 Marginally stable inviscid flows with critical layers. *IMI J. Appl. Maths* **27**, 133–173.

TAM, C. K. M. & HU, F. Q. 1989 Instabilities of supersonic mixing layers inside a rectangular channel. *AIAA J.* (submitted).